HHS Public Access

Author manuscript

Anal Bioanal Chem. Author manuscript; available in PMC 2019 May 01.

Published in final edited form as:

Anal Bioanal Chem. 2018 May ; 410(14): 3385–3394. doi:10.1007/s00216-018-1034-6.

Simple and Inexpensive Micromachined Aluminum Microfluidic Devices for Acoustic Focusing of Particles and Cells

Gayatri P. Gautam[1], **Tobias Burger**[2], **Andrew Wilcox**[2], **Michael J. Cumbo**[3], **Steven W. Graves**[4], and **Menake E. Piyasena**[1,*]

[1]Department of Chemistry, New Mexico Institute of Mining and Technology, 801 Leroy Pl., Socorro, NM 87801, USA

[2]Department of Chemical Engineering, New Mexico Institute of Mining and Technology, Socorro, NM 87801, USA

[3]Eta Diagnostics, Albuquerque, NM 87107, USA

[4]Center for Biomedical Engineering & Department of Chemical and Biological Engineering, University of New Mexico, Albuquerque, NM 87131, USA

Abstract

In this work, we introduce a new method to construct microfluidic devices especially useful for bulk mode acoustic wave (BAW) based manipulation of cells and microparticles. In order to obtain an efficient acoustic focusing, BAW devices require materials that have high acoustic impedance mismatch relative to the medium that cells/microparticles are suspended within and materials with a high-quality factor. To date, silicon and glass have been the materials of choice for BAW based acoustofluidic channel fabrication. Silicon and glass based fabrication is typically performed in clean room facilities, generate hazardous wastes, and can take several hours to complete the microfabrication. To address some of the drawbacks in fabricating conventional BAW devices, we explored a new approach by micromachining microfluidic channels in aluminum substrates. Additionally, we demonstrate plasma bonding of PDMS onto micromachined aluminum substrates. Our goal was to achieve an approach that is both low-cost and effective in BAW applications. To this end, we have micromachined Aluminum 6061 plates and enclosed the systems with a thin PDMS cover layer. These aluminum/PDMS hybrid microfluidic devices use inexpensive materials and are simply constructed outside of a clean room environment. Moreover, these devices demonstrate effectiveness in BAW applications as demonstrated by efficient acoustic focusing of polystyrene microspheres, bovine red blood cells, and Jurkat cells and generating multiple focused streams in flow through systems.

Graphical Abstract

*Corresponding Author: sesathpura.piyasena@nmt.edu.

Compliance with ethical standards

Conflict of interest

Gayatri P. Gautam, Tobias Burger, Andrew Wilcox, and Menake E. Piyasena declare that they have no conflict of interest. Steven W. Graves and Michael J. Cumbo would like to declare a commercial interest in this technology as it is relevant to their commercial company, Eta Diagnostics, which is commercializing parallel acoustic flow cytometers.

A composite figure showing the aluminum acoustofludic device and the generation of multinode focusing of particles.

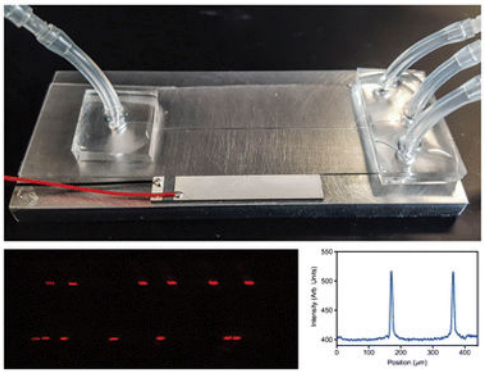

Keywords

Micromachining; Microfluidics; Acoustic Focusing; PDMS; Aluminum

Introduction

Acoustic standing waves provide a fast, non-contact, and gentle particle manipulation technique in microfluidic conditions. It has emerged as a promising new microfluidic technology for purification, separation, and concentration of beads and biological cell samples [1–10]. Acoustofluidic devices are routinely fabricated on silicon, glass, or poly(dimethylsiloxane) (PDMS) substrates [1, 8–12]. The device material and the format of focusing are mainly governed by the type of acoustic waves, either bulk or surface, being used. In the bulk acoustic wave (BAW) mode, acoustic waves are generated inside the microchannel resonant chamber and in the surface acoustic wave (SAW) mode, acoustic waves are generated on the surface of a substrate that is adhered to the microchannel [13–18].

In SAW devices, interdigital transducers (IDT) are fabricated on a piezoelectric surface to generate standing waves and often poly(dimethylsiloxane) (PDMS) microchannels are adhered on to the piezoelectric substrate [9, 13, 19]. Because SAW devices do not rely on resonant chambers, soft polymers like PDMS can be used as microchannel material. PDMS microchannels can easily be adhered onto the piezoelectric surface via plasma bonding. However, fabrication of electrodes on the piezoelectric surface needs to be precise and expensive equipment are needed for mask alignment and electrode metal deposition. Often, this equipment is housed in dedicated clean room facilities.

On the other hand, BAW devices rely on resonant chambers with parallel rigid walls that are capable of reflecting acoustic waves with minimum loss, therefore; the device substrate should possess high acoustic impedance and high Q-value (quality factor) [18]. Soft polymer materials like PDMS are not suitable for BAW, as the polymer walls of such devices lack the necessary difference in acoustic impedance (as compared to the aqueous solution) and acoustic damping is high [11, 20]. Materials with good acoustic properties (higher Q-value,

density, speed of sound, and high impedance) are needed to construct effective BAW devices.

To date, silicon and glass have been the materials of choice for BAW based acoustofluidic channel fabrication. The process has several complex and costly steps that require dedicated instruments like mask aligner and deep reactive ion etcher and/or hazardous materials if chemical etching is used. Many of these steps are carried out in clean room facilities and it is a time consuming and expensive process. Commercially available rectangular or square glass micro-capillaries can also be used to create acoustofluidic devices [12, 21]. However, this approach is not amenable to design complex devices with multiple inlets and outlets and the dimensional tolerances are not precise (typically +/− ~10% of the dimension in question). Recently, microchannels fabricated on thermoplastic (polystyrene) have been utilized in acoustic separation of particles and cells. The biocompatibility of the thermoplastic substrate is attractive for many biological applications, however, due to high acoustic attenuation of the material, acoustic transducers are driven at a very high voltage (~80 V) and these systems need an efficient cooling mechanism [22, 23].

To address many of the drawbacks in fabricating BAW devices, we explored a new approach by micromachining microfluidic channels in aluminum substrates. Additionally, we demonstrate plasma bonding of PDMS onto micromachined aluminum substrates, which provides a quick and convenient way of enclosing metallic microchannel structures for fluidic applications. Our method does not require photolithography, clean room facilities, or etching thus eliminating long process times, hazardous reagents, and specialized equipment. Microchannels can easily be machined using widely available commercial machining equipment. There has been only one prior report of fabricating a microfluidic device via micromachined aluminum [24]. However, their approach was not simple and comprised of a glass window sandwiched between an epoxy block and a micromachined aluminum block and these layers were assembled using screws. Further, liquid access ports were machined horizontally through the aluminum substrate and rigid plastic connectors were screwed to each liquid port causing limited flexibility in designing more complex microchannel patterns. The device was bulky and not amenable for customization. The process we have developed is rapid, simple, and inexpensive and it can be done at most micromachining facilities. While we expect these devices will be useful in general for microfluidic applications, our implementation in aluminum based devices has specific relevance for BAW applications. Aluminum exhibits a high acoustic impedance relative to aqueous solutions typically of interest in acoustofluidic applications [18, 25]. The efficacy of this new method is demonstrated via acoustic focusing of microspheres and cells in single and multinode acoustic focusing modes.

Experimental

Materials

Aluminum (6061 alloy) plates were purchased from McMaster-Carr (Los Angeles, CA) and Poly(dimethylsiloxane) (PDMS) was purchased from Ellsworth Adhesives (Germantown, WI). Silicone tubing (0.64 mm ID) were purchased from Cole Parmer (Vernon Hills, IL). PZT ceramic transducers were purchased from APC International Ltd (Mackeyville, PA).

Acetone, PBS buffer tablets, and casein were purchased from Sigma Aldrich (St. Louis, MO). Bovine red blood cells (B-RBCs) were purchased from Innovative Research (Novi, MI). Nile red polystyrene particles (NR-ps) were purchased from Spherotech (Lake Forest, IL) and CountBright™ absolute counting beads were purchased from Life Technologies (Carlsbad, CA).

Micromachining of the acoustofluidic device

Two, 7 cm long microfluidic flow channels with trifurcated outlets (Fig. 1a), one with 250 μm wide main channel and another with 430 μm wide main channel were designed using AutoCAD software (Autodesk, San Rafael, CA). In order to demonstrate the feasibility of using any machining facility for microchannel micromachining, aluminum substrates were milled at two different local machining facilities. The CAD design was feed to the computer connected to a CNC machine (HAAS VF-2-super speed, Haas Automation Inc., Oxnard, CA or Bed Mills with Centroid Control, Birmingham). An 80 μm deep channel was milled into a thin (5 mm) aluminum substrate using a high-speed end mill fitted into the CNC.

Plasma sealing of PDMS onto Al substrate

The micromachined channel (Fig. 1a) was enclosed for fluid flow by sealing a thin PDMS film to the top of the channel (Fig. 1b). First, a PDMS film with a thickness of ~10–15 μm was prepared by spin coating an uncured PDMS mixture onto a thin transparency plastic (Mylar™) sheet at 500 rpm for 1 minute. The PDMS film was then allowed to cure in an isothermal oven at 65 °C for 15–30 min. Next, the micromachined aluminum substrate (Al device) was thoroughly cleaned with acetone and iso-propanol followed by rinsing with de-ionized water and drying under a stream of compressed nitrogen gas. Next, the device was heated to 140 °C on a hot plate for 2–3 minutes to ensure the complete dryness and the cleaned Al device and the cured PDMS film were exposed to air plasma (Harrick Plasma, Ithaca, NY) for 30 seconds and bonded together. The bonding was allowed to set for about 2–3 hours at ~ 25 °C. Next, the plastic transparency sheet was carefully peeled off from the bonded PDMS film and the film was punched at the two ends of the channel for fluid inlets and outlets using Harris Uni-Core punches (Ted Pella, Redding, CA).

Device preparation for acoustic focusing

Two-centimeter long silicone tubing were attached to each inlet and outlet of the enclosed microchannel for liquid connection by applying non-cured PDMS as a glue and letting it cure at 65 °C for 2–3 minutes (Fig. 1c). Finally, a lead zirconium titanate (PZT) acoustic transducer (30 mm long, 5 mm wide) with an optimum frequency of 2.91 MHz was super-glued to the top or to the bottom surface of the final device (Fig. 2a–d) to implement acoustic wave fields. The frequency of the PZT was chosen based on microchannel's half width.

Surface roughness and device variation analysis

The surface roughness and the batch-to-batch variations of the device width were investigated via SEM imaging (Nova NanoSEM™450) while width and depth variation was investigated via optical profilometer scanning (Zygo ZeGage™) (Fig 3a–c). A minimum of

three devices was used for the comparison. SEM images were taken at the center of the main channel along the longitudinal direction and the profilometer scanning was taken at three random positions along the main channel.

Flow and pressure measurements in Al devices

The maximum flow rate and the pressure that the device can withstand were evaluated by continuous flowing of PBS buffer at an increasing flow rate and pressure. For flow rate measurements, the inlet of the device was connected to a syringe pump (KD Scientific, MA) and fluid was flowed at a set flow rate for about 5 minutes, starting at 25 μL/min. The flow rate was then gradually increased by 25 μL/min increment until the final flow rate of 4 mL/min. We assumed the volumetric flow rate inside the channel was same as the flow rate set at the syringe pump. For pressure measurements, the pressure at the outlet was monitored via a digital pressure gauge (DPG1000B, Omega, Norwalk, CT) connected to the device outlet while the flow rate was gradually increased.

Acoustic focusing of microspheres and cells

To demonstrate the performance of the aluminum device, a series of typical acoustic focusing experiments were carried out. First, we show the single node focusing of particles by focusing polystyrene particles and biological cells and second, we demonstrate the multinode focusing of particles by focusing particles into two parallel streams. Devices were first rinsed with 1% casein solution followed by 10 mM PBS buffer (pH 7.5) to minimize the non-specific adhesion of particles and cells to the channel walls. A sample of polystyrene particles (10^5 particles/mL) was prepared by diluting a stock solution of fluorescent NR-ps particles in 20 mL of PBS buffer. For cell samples, Nile red stained Jurkat cells and B-RBCs were used. To stain, 1 mL of Jurkat cells (~10^6/mL) was mixed with 5 μL of Nile red solution (in DMSO). For B-RBCs, the original sample obtained from the vendor was diluted 200 folds and 1 mL of the diluted sample was stained with 5 μL Nile red without further quantification. Each sample was then diluted to 5 mL with PBS buffer and excess Nile red in the cell suspension was removed by discarding the supernatant after centrifugation. The stained cell sample was then re-suspended in 5 mL of 10 mM PBS buffer. Samples were introduced to the device at a flow rate of 100 μL/min using a syringe pump (KD Scientific, MA). The resonance standing acoustic waves were generated using a waveform generator (RIGOL DG 1022, RIGOL Technologies Inc., OR) and amplified via an RF amplifier (E&I 350L, Electronics & Innovation Ltd., NY). The acoustic performance parameters (frequency, applied voltage, amplitude) were monitored via an oscilloscope (Tektronix TBS 1052B, Tektronix Inc., OR).

Fluorescence imaging and flow cytometry analysis

Acoustic focusing of particles and cells in the aluminum device was monitored via epi-fluorescence imaging and the extent of the focusing was measured via flow cytometry. The epi-fluorescence images and videos of particle streams were captured near to the end of PZT using an epi-fluorescence microscope equipped with a sCMOS camera (Orca-FLASH 4.0, Hamamatsu, Japan). The obtained images were analyzed by plot profile scanning using ImageJ software (NIH) to compare intensity and resolution profiles of focused and non-focused streams. In addition, 1 mL sample was collected from each outlet and analyzed via a

BD FACSCalibur flow cytometer to determine the concentrations of particles in each fluid stream, prior and during the acoustic focusing. In order to determine the particle concentration in each sample, an internal calibration method was employed using flow cytometry standard beads. Briefly, 950 μL of bead sample collected from an outlet was mixed with 50 μL of concentration known CountBright™ absolute counting beads. The concentration of particles or cells was calculated via flow cytometry dot plots, using the following equation.

$$Concentration\,(per\,mL) = \left(\frac{\#\ of\ particle\ events}{\#\ of\ standard\ bead\ events}\right)\left(\frac{Standard\ beads\ in\ total\ volume}{Total\ volume\,(mL)}\right)$$

The flow cytometry counting beads have a distinct signal from particles used, hence, two regions of particles were appeared in the dot plots (see Electronic Supplementary Material (ESM) Fig. S1). Pure samples of NR-ps particles were first measured to define the regions of interest for test particles in each dot plot and defined the gates accordingly. All particle populations were gated based on their fluorescence intensities (via FL2 fluorescence channel of the flow cytometer that detects the fluorescence at 585 ± 21 nm) and side scattering and the data were presented in the form of dot plots of side scatter (SSC) vs. fluorescence intensity (FL2). All data collection and analysis were performed using BD CellQuest™Pro (BD Bioscience, San Jose, CA) and FCS Express 6 (De Novo Software, Glendale, CA) software respectively. Total of 10,000 events was measured in each measurement and the instrument threshold was set at FL2 to remove unwanted events resulting from non-analytes.

Results and discussion

Construction of the acoustofluidic device in aluminum

While metal micromachining has not been a common method for microfluidic device construction, the routine availability of mills with very high RPM heads and the development of micro end mills as small as 1 μm cutting diameter is making this approach a compelling method to create micro channels even smaller than 25 μm in width. Among the different grades of aluminum, the alloy 6061 (AL6061) is inexpensive, readily available, corrosion resistant, and highly machinable. The speed of sound in AL6061 is 6320 m/s (vs. 1482 m/s in water), which assures a high acoustic impedance mismatch between microchannel walls (17.06×10^6 kg m^{-2} s^{-1}) and the aqueous solutions (water ~ 1.48×10^6 kg m^{-2} s^{-1}) in the channel [18, 25]. This is particularly useful in bulk acoustofluidic devices that require a rigid material to serve as an efficient carrier of acoustic energy that is launched into the channel to create a resonance acoustic field within the fluid. In comparison, silicon substrates commonly used for fabrication of acoustofluidic devices, have an acoustic impedance of 19.79×10^6 kg m^{-2} s^{-1} [18], which is slightly better than Al substrates, however the easy access of micromachining facilities, non-clean room requirement, and the low cost of fabrication will compel the use of aluminum as an alternate for silicon. Further, Al is a better thermal conductor (~167 W/m K) in comparison to semiconductor glass (~12 W/m K) and silicon (~148 W/m K). The thermal stability is important to maintain stable resonance frequency in acoustofluidic systems. Further, micro-machining of aluminum devices is much faster than microfabrication of silicon devices. For example, we could

micro-machine the device reported in the current study, in less than an hour, whereas silicon microfabrication of similar device can take up to three hours or more. For comparison, we used two micromachining facilities; a commercial source and the on-campus facility and we did not observe significant differences in quality of the final product or the efficiency of acoustic focusing. The fabricated aluminum device was operated in the transverse resonator mode, where the standing acoustic waves were obtained perpendicular to the incident direction [18].

To provide a straightforward method to introduce samples and reagents, the liquid ports were integrated perpendicular to the microfluidic channel. This approach is simple and convenient in comparison to the method reported by Lin et al. where liquid access ports were micromachined horizontally through a thick aluminum substrate, which limits the number of liquid ports that can accommodate thus limiting the microfluidic design to simple geometries [24]. Further, a thick substrate is necessary to accommodate horizontal through ports which is not favorable for acoustic applications. Our design is not limited by the substrate thickness and can be further improved by utilizing aluminum sheets as thin as 300–500 μm which is comparable to the thickness of most common silicon wafers. In the current work, the challenge in integrating liquid ports onto metal surfaces is overcome by plasma sealing of PDMS onto Al substrates, a simple process, and it does not deviate from conventional silicon-PDMS plasma sealing procedure. Silicone tubing for liquid access can then be conveniently mounted onto the plasma-bonded PDMS layer. For acoustofluidic applications, it is essential to use a thin film of PDMS in order to minimize attenuation of acoustic forces by the polymer substrates; however, we found out that it is possible to plasma seal thick PDMS slabs as well.

The presence of smooth microchannel walls is vital to minimize unwanted particle adhesion. The surface smoothness of aluminum devices was compared to that of silicon devices prepared via deep reactive ion etching, simply by comparing the SEM images of channel surfaces of two devices (Fig. 3). Even though visual analysis of SEM images may not be the most perfect way to compare the roughness; the qualitative information we could gather should provide adequate information for the comparison. The two SEM images of the Al (Fig. 3a) and the silicon (Fig. 3b) devices suggest that the surface of the DRIE silicon channel appears smoother than the surface of the aluminum device, however, the aluminum channel surface was smooth enough that we did not observe any impact on the device performance (i.e. no particle sticking, loss of focusing, variation in resonance frequency). The profilometer measurement indicates that more precise micromachining of Al substrate, by having a mean width of three finished channels (433 ±12 μm) near to the target width (430 μm), in comparison to DRIE channel, where, we observed an average of ~12% expansion in the width (+30 μm) of the silicon channel from the target width of 250 μm. We used photomask printed on plastic Mylar™ (20,000 dpi) for photolithography during DRIE. The precision of DRIE channels can be improved if chrome masks are used, however, this can be expensive. Thus, no need of expensive photomask is another attractive feature of aluminum devices. The average depth of aluminum channel was about 80 ± 6 μm (target depth = 80 μm). The microchannels fabricated at the on-campus facility were milled at 3000 rpm. The precision and smoothness of the microchannels can be further improved by optimizing the rpm of the spindle speed and the feed rate. CNC machines that are capable of

operating at higher spindle speed can produce high precision and smoother microchannels [26].

The ability to hold high flow rates and pressures without rupturing the bonded polymer film or delaminating the Al-PDMS composite was evaluated by flowing PBS buffer at increasing flow rates. We tested up to 4 mL/min and we did not observe delamination or rupturing of the PDMS film. The recorded highest hydrostatic pressure at this maximum flow rate was 4.5 atm. The thin film was also robust for repeated usage at high flow rates and the film was not ruptured even after 25-repeated use of the device. Another advantage of having a polymer layer is that it can be taken out by scraping. The device can then be cleaned with organic solvents and rebuild for extended use.

Device configuration for optimum acoustic focusing

The placement of the acoustic transducer to generate resonance standing waves can be varied [6, 27, 28]. In most silicon based BAW devices, the acoustic transducer is attached to the bottom of the channel. For aluminum devices, we found that this configuration yields very weak focusing of particles. Therefore, we explored several possible configurations of transducer attachment to generate the most effective acoustic focusing. The effectiveness was determined by focusing 10.2 μm NR-ps particles at an applied voltage of 18 $V_{P\text{-}P}$ while changing the fluid flow rate. The device was running in single node mode and a frequency scan (2.5–3.5 MHz) was performed to obtain the optimum resonance frequency of the device. Epi-fluorescence images were taken at each tested flow rate at the optimum frequency for the analysis. The focusing efficiency was determined via plot profile scanning of images using ImageJ software. If the full width at half maximum (FWHM) of the focused stream peak was less than 30 μm, the focusing was deemed efficient (data not presented).

In the first configuration, in addition to the plasma bonded PDMS film, a glass cover slide was also plasma bonded to the top of the PDMS film and the PZT transducer was adhered on top of that using a thin layer of epoxy glue (Fig. 2a). The purpose of having the glass cover slide was that we anticipated the soft PDMS thin film would attenuate acoustic field strength and by having a glass substrate would provide a rigid acoustic reflector that can minimize the acoustic attenuation. However, we did not observe acoustic focusing of particles in this configuration.

In the second configuration, there was no glass cover slide on the PDMS film and the PZT was attached to the bottom surface of the aluminum substrate, positioned parallel and directly underneath to the channel (Fig. 2b). We observed weak acoustic focusing of particles when the flow rate was low (<15 μL/min). The focusing was not reproducible thus we considered the acoustic focusing as inefficient. The 5 mm thickness and/or mass of the aluminum substrate, which is large compared to silicon wafers that are typically 500 μm thick, could have attenuated the strength of acoustic vibrations reaching the microchannel and resulted inefficient acoustic focusing of particles in this configuration. Additionally, the design of acoustic horns, which the aluminum layer is analogous to here, requires precise calculation to match thickness of the material. This was not done in this configuration and matching the thickness of the aluminum layer to these calculations might improve device performance.

In the third configuration (Fig. 2c), a similar device as in the second configuration was built and the only difference was the placement of the PZT. The PZT was attached to the top surface of the aluminum layer of the device, positioned adjacent and parallel to the microchannel (Fig. 2c and 2d). Here, we observed stronger, reproducible focusing of NR-ps even at comparatively higher flow rates (~100 μL/min) than in other configurations. We anticipate the improved performance is related to the close proximity of the PZT transducer to the flow channel. The optimum resonance frequency was found to be 3.13 MHz and the driving voltage necessary to acquire efficient focusing was between 18–20 $V_{p\text{-}p}$. The captured video shows the real time focusing of NR-ps in the device taken at a flow rate of 100 μL/min (ESM Movie S1).

Acoustic focusing of microspheres and cells

Acoustic focusing performance of the aluminum device was demonstrated via a set of typical acoustic focusing experiments. The data in Figure 4a–c are obtained from the single node acoustic focusing of 10.2 μm diameter NR-ps particles in the 250 μm wide channel, at a flow rate of 100 μL/min. and at an applied voltage of 18.6 V_{pp}. The Figure 4a (left) shows a stream of particles flowing through the channel in the absence of an applied acoustic field and the plot profile image scan (Fig. 4a, right) shows the appearance of random peaks due to unfocused particles in the fluid stream. In Figure 4b (left), particles are focused into a single streak in the presence of an acoustic field at 3.13 MHz. The plot profile scanning of the epi-fluorescence image shows the appearance of single focused peak with a FWHM of 18 μm (Fig. 4b, right), which is less than a $1/10^{th}$ of the width of the channel, suggesting a very good focusing of particles into the center of the channel (ESM movie S1). In order to quantify the focusing efficiency, the percentages of particle concentrations in the central stream and the combined lateral streams were compared via flow cytometry analysis. The internal standard beads were utilized to calculate the percentages of particles in each stream as described in the experimental section. Initially, in the absence of acoustic focusing, the two lateral streams contained 54.3% of the total collected particles (Fig. 4c). In the presence of acoustic forces, the central stream is significantly concentrated with particles thus changing the particle composition from 45.7% to 98.2% of total collected. Once we established that our aluminum devices are capable of focusing particles efficiently, we explored the capability of focusing biological samples. For the proof of the concept study we utilized fluorescently labeled B-RBCs (Fig. 5, ESM Movie S2) and Jurkat cells (ESM, Fig. S2 and Movie S3). In the absence of an applied acoustic field, B-RBCs are dispersed across the channel width as shown in the epi-fluorescence micrograph (Fig. 5a) as well as its plot profile scanning (Fig. 5b), once the resonance acoustic field is applied B-RBCs are focused (Fig. 5c and d). The stained B-RBCs have weak fluorescence as indicated by the Figure 5a, however, when focused, the overall fluorescence intensity is greatly enhanced (Fig. 5c). The FWHM of the focused stream is about 34 μm, which is slightly higher than the threshold FWHM (30 μm) of a peak of pre-defined efficient focusing. As the Figure 5c suggests, the B-RBCs are highly concentrated in the tested sample and the focusing could have been improved either by diluting the initial cell sample or by increasing the applied voltage. Nevertheless, data suggest that our aluminum based acoustofluidic devices are capable of focusing biological cells of micrometer size.

One of the key advantages of acoustic focusing in microfluidic devices is its ability to generate multiple focused streams of particles in a single microfluidic channel without having complex designs, by simply tuning the resonance frequency to generate multiple nodes [12, 21]. To explore the feasibility of generating parallel focused particle streams in our aluminum devices, 10.2 μm NR-ps particles were focused into two streams at a resonance frequency of 3.43 MHz and flow rate of 100 μL/min in a 440 μm wide channel (ESM Movie S4). The multinode focusing was monitored microscopically (Fig. 6a and c) and captured images were analyzed (Fig. 6b and d). The Figure 6d shows that these devices are capable of delivering multi node focusing at commonly used voltages (18–20 V). The two particle streams are focused tightly with FWHM of about 10 μm for both peaks. The data shown in Figure 6c suggests that two nodes are not symmetrically positioned across the width of the microchannel and this non-symmetry can be due to the existence of three dimensional acoustic fields resulting from the vibration of the whole device [29]. It has been reported that the confinement of the resonance wave to a particular channel geometry can be influenced not only by the geometry and acoustic properties of the channel substrate but also by the properties of supporting layers [29, 30]. A thorough study is necessary to characterize acoustic fields in aluminum based devices.

Conclusions

The focus of this work has been to demonstrate the fabrication of aluminum based microfluidic devices and the feasibility of using them in BAW applications. Silicon, glass, and PDMS have been well established as materials of choice for making microfluidic devices. These materials encompass proper properties needed for microfabrication of microfluidic channels. Metals as microfluidic channel substrates are not commonly used. This can be due to the difficulty in the integration of fluidic connection in order to introduce samples and reagents. However, bonding of PDMS substrates to metal surfaces can resolve issues in fluidic integration. We have demonstrated that PDMS can be strongly bonded to micromachined aluminum microchannels. The aluminum alloy 6061 is reactive in strong acidic and basic conditions, however, most microfluidic systems are operated at neutral or near neutral conditions (pH 6–8), where the aluminum 6061 is non-reactive. Aluminum microchannels are especially useful for BAW applications, in addition to good acoustic properties, aluminum micromachining is inexpensive and widely available. The method we have reported here is simple and has fewer steps than silicon microfabrication and it does not require harsh chemicals and does not generate hazardous waste. Complex microchannel structures can be micromachined on AL6061. Further, aluminum devices can be machined at any standard micromachining facility and the overall cost for bulk machining will be less than other microfluidic fabrication methods. Finally, we have shown the usefulness of these devices in acoustofluidic applications, by efficient focusing of polystyrene microspheres and biological cells in single and multinode format. The general availability, the low cost, and the effectiveness for BAW applications will make this approach of value to researchers in a wide variety of fields and for a number of applications that include acoustophoretic separations, acoustic flow cytometry, and acoustic trapping among others. Aluminum based microfluidic devices need to be further explored and improved for a variety of applications and we anticipate this initial work will eventually be expanded.

Supplementary Material

Refer to Web version on PubMed Central for supplementary material.

Acknowledgments

Menake E. Piyasena would like to acknowledge funding for an Institutional Development Award (IDeA) from the National Institute of General Medical Sciences of the National Institutes of Health under grant number P20GM103451 and Steven W. Graves would like to acknowledge funding from NIH R21GM107805 and NSF 1130140. Steven W. Graves and Michael J. Cumbo acknowledge funding from NIH R44GM117649. The authors thank Dr. Snezna Rogelj and Danielle Turner in the department of biology at NMT for providing Jurkat cell samples. The authors also thank Esequiel Lopez of Sandia Electro-Optics Corporation for his work and assistance with the machining of the devices and Dr. Paul Fuierer and Robert Calvo in the materials engineering department at NMT for their help with profilometer measurements. This work was performed, in part, at the Center for Integrated Nanotechnologies (CINT), an Office of Science User Facility operated for the U.S. Department of Energy (DOE) Office of Science by Los Alamos National Laboratory (Contract DE-AC52-06NA25396) and Sandia National Laboratories (Contract DE-NA-0003525). Authors would like to thank Douglas V. Pete at CINT, Albuquerque for the assistance in obtaining SEM images. Steven W. Graves and Michael J. Cumbo would like to declare a commercial interest in this technology as it is relevant to their commercial company, Eta Diagnostics, which is commercializing parallel acoustic flow cytometers.

References

1. Shi J, Huang H, Stratton Z, Huang Y, Huang TJ. Continuous particle separation in a microfluidic channel via standing surface acoustic waves (SSAW). Lab Chip. 2009; 9(23):3354–9. [PubMed: 19904400]
2. Petersson F, Nilsson A, Holm C, Jonsson H, Laurell T. Continuous separation of lipid particles from erythrocytes by means of laminar flow and acoustic standing wave forces. Lab Chip. 2005; 5(1):20–2. [PubMed: 15616735]
3. Hawkes JJ, Barber RW, Emerson DR, Coakley WT. Continuous cell washing and mixing driven by an ultrasound standing wave within a microfluidic channel. Lab Chip. 2004; 4(5):446–52. [PubMed: 15472728]
4. Johansson L, Nikolajeff F, Johansson S, Thorslund S. On-chip fluorescence-activated cell sorting by an integrated miniaturized ultrasonic transducer. Anal Chem. 2009; 81(13):5188–96. [PubMed: 19492800]
5. Yasuda K, Haupt SS, Umemura S-i, Yagi T, Nishida M, Shibata Y. Using acoustic radiation force as a concentration method for erythrocytes. J Acoust Soc Am. 1997; 102(1):642–5. [PubMed: 9228824]
6. Haake A, Neild A, Kim DH, Ihm JE, Sun Y, Dual J, et al. Manipulation of cells using an ultrasonic pressure field. Ultrasound Med Biol. 2005; 31(6):857–64. [PubMed: 15936501]
7. Petersson F, Nilsson A, Holm C, Jonsson H, Laurell T. Separation of lipids from blood utilizing ultrasonic standing waves in microfluidic channels. Analyst. 2004; 129(10):938–43. [PubMed: 15457327]
8. Goddard G, Martin JC, Graves SW, Kaduchak G. Ultrasonic particle-concentration for sheathless focusing of particles for analysis in a flow cytometer. Cytometry A. 2006; 69(2):66–74. [PubMed: 16419065]
9. Ai Y, Sanders CK, Marrone BL. Separation of Escherichia coli bacteria from peripheral blood mononuclear cells using standing surface acoustic waves. Anal Chem. 2013; 85(19):9126–34. [PubMed: 23968497]
10. Lenshof A, Jamal A, Dykes J, Urbansky A, Åstrand - Grundström I, Laurell T, et al. Efficient purification of CD4+ lymphocytes from peripheral blood progenitor cell products using affinity bead acoustophoresis. Cytometry A. 2014; 85(11):933–41. [PubMed: 25053536]
11. Evander M, Lenshof A, Laurell T, Nilsson J. Acoustophoresis in wet-etched glass chips. Anal Chem. 2008; 80(13):5178–85. [PubMed: 18489126]

12. Austin Suthanthiraraj PP, Piyasena ME, Woods TA, Naivar MA, Lopez GP, Graves SW. One-dimensional acoustic standing waves in rectangular channels for flow cytometry. Methods. 2012; 57(3):259–71. [PubMed: 22465280]
13. Shi J, Mao X, Ahmed D, Colletti A, Huang TJ. Focusing microparticles in a microfluidic channel with standing surface acoustic waves (SSAW). Lab Chip. 2008; 8(2):221–3. [PubMed: 18231658]
14. Laurell T, Petersson F, Nilsson A. Chip integrated strategies for acoustic separation and manipulation of cells and particles. Chem Soc Rev. 2007; 36(3):492–506. [PubMed: 17325788]
15. Yeo LY, Friend JR. Ultrafast microfluidics using surface acoustic waves. Biomicrofluidics. 2009; 3(1):012002–23.
16. Friend J, Yeo LY. Microscale acoustofluidics: Microfluidics driven via acoustics and ultrasonics. Rev Mod Phys. 2011; 83(2):647–704.
17. Gedge M, Hill M. Acoustofluidics 17: Theory and applications of surface acoustic wave devices for particle manipulation. Lab Chip. 2012; 12(17):2998–3007. [PubMed: 22842855]
18. Lenshof A, Evander M, Laurell T, Nilsson J. Acoustofluidics 5: Building microfluidic acoustic resonators. Lab Chip. 2012; 12(4):684–95. [PubMed: 22246532]
19. Franke T, Braunmuller S, Schmid L, Wixforth A, Weitz DA. Surface acoustic wave actuated cell sorting (SAWACS). Lab Chip. 2010; 10(6):789–94. [PubMed: 20221569]
20. Bora M, Shusteff M. Efficient coupling of acoustic modes in microfluidic channel devices. Lab Chip. 2015; 15(15):3192–202. [PubMed: 26118358]
21. Piyasena ME, Austin Suthanthiraraj PP, Applegate RW, Goumas AM, Woods TA, Lopez GP, et al. Multinode acoustic focusing for parallel flow cytometry. Anal Chem. 2012; 84(4):1831–9. [PubMed: 22239072]
22. Mueller A, Lever A, Nguyen T, Comolli J, Fiering J. Continuous acoustic separation in a thermoplastic microchannel. J Micromech Microeng. 2013; 23(12):125006.
23. Dow P, Kotz K, Gruszka S, Holder J, Fiering J. Acoustic separation in plastic microfluidics for rapid detection of bacteria in blood using engineered bacteriophage. Lab Chip. 2018; doi: 10.1039/C7LC01180F
24. Lin Y-S, Huang K-S, Hsieh W-C. An aluminum microfluidic chip fabrication using a convenient micromilling process for fluorescent poly(DL-lactide-co-glycolide) microparticle generation. Sensors. 2012; 12:1455–67. [PubMed: 22438719]
25. Eghtesad A, Knezevic M. A new approach to fluid–structure interaction within graphics hardware accelerated smooth particle hydrodynamics considering heterogeneous particle size distribution. Comp Part Mech. 2017; doi: 10.1007/s40571-017-0176-1
26. Jahanmir S. Surface integrity in ultrahigh speed micromachining. Procedia Eng. 2011; 19:156–61.
27. Wiklund M, Gunther C, Lemor R, Jager M, Fuhr G, Hertz HM. Ultrasonic standing wave manipulation technology integrated into a dielectrophoretic chip. Lab Chip. 2006; 6(12):1537–44. [PubMed: 17203158]
28. Nilsson A, Petersson F, Jonsson H, Laurell T. Acoustic control of suspended particles in micro fluidic chips. Lab Chip. 2004; 4(2):131–5. [PubMed: 15052353]
29. Manneberg O, Melker Hagsäter S, Svennebring J, Hertz HM, Kutter JP, Bruus H, et al. Spatial confinement of ultrasonic force fields in microfluidic channels. Ultrasonics. 2009; 49(1):112–9. [PubMed: 18701122]
30. Hagsater SM, Jensen TG, Bruus H, Kutter JP. Acoustic resonances in microfluidic chips: full-image micro-PIV experiments and numerical simulations. Lab Chip. 2007; 7(10):1336–44. [PubMed: 17896019]

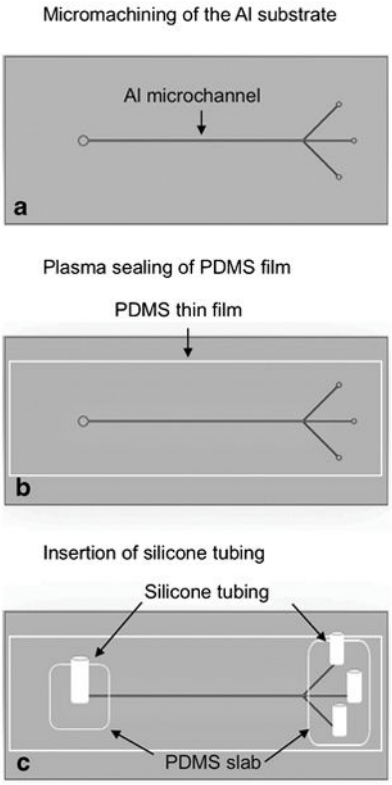

Fig. 1.

The fabrication steps of an aluminum acoustofluidic device. A microchannel is micromachined on aluminum alloy 6061 (a) followed by sealing of a PDMS film to enclose the channel (b) and insertion of silicone tubing for liquid connection (c).

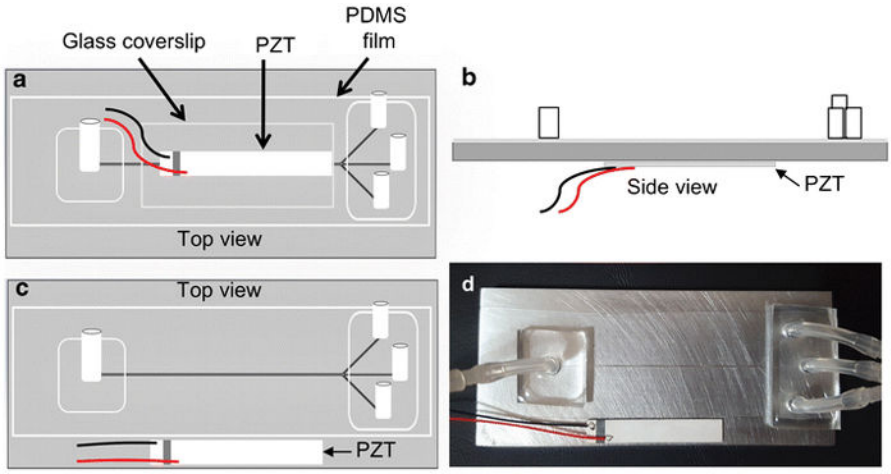

Fig. 2.

The schematic diagrams showing three approaches of the placement of the acoustic transducer (a–c) and the image of the working device (d). The PZT is glued to the glass cover slip on top of a plasma sealed PDMS film (a). The PZT is glued to the bottom surface of the Al substrate (b). The PZT is glued to the top surface of the Al substrate, parallel to the machined microchannel (c). Final working device with the configuration shown in (c) (d).

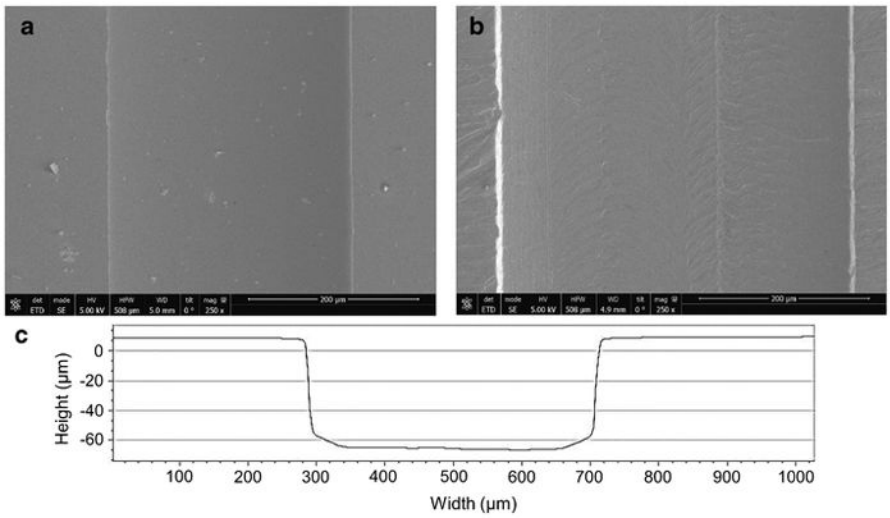

Fig. 3.

SEM Images of micromachined aluminum device (a) and deep reactive ion etched silicon device (b) for the comparison of surface smoothness. These images were taken near to the center of the channel in longitudinal direction. The optical profilometer scanning of the aluminum device showing the vertical and parallel walls (c).

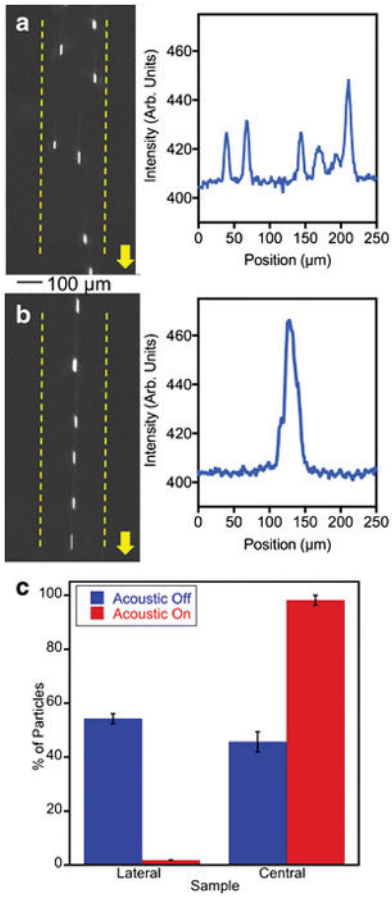

Fig. 4.

The single node acoustic focusing of polystyrene microspheres in the micromachined Al device (width =250 μm). Non-focused (a) and focused stream (b) of 10.2 μm Nile red particles and their respective plot profiles on right. Bar graphs indicating the efficiency of separation obtained from flow cytometry quantification (c).

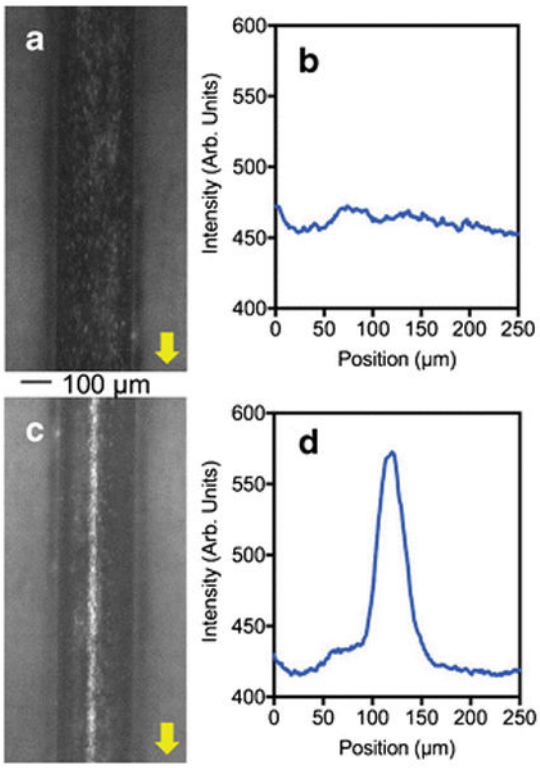

Fig. 5.

Epi-fluorescence micrographs and the plot profile image scanning showing the acoustic focusing of bovine red blood cells in micromachined Al device. Nile red stained bovine RBCs in the absence of acoustic force (a) and its plot profile image scanning obtained from ImageJ software (b). The focused bovine RBCs in the presence of resonance acoustic waves (c) and its plot profile image scanning (d).

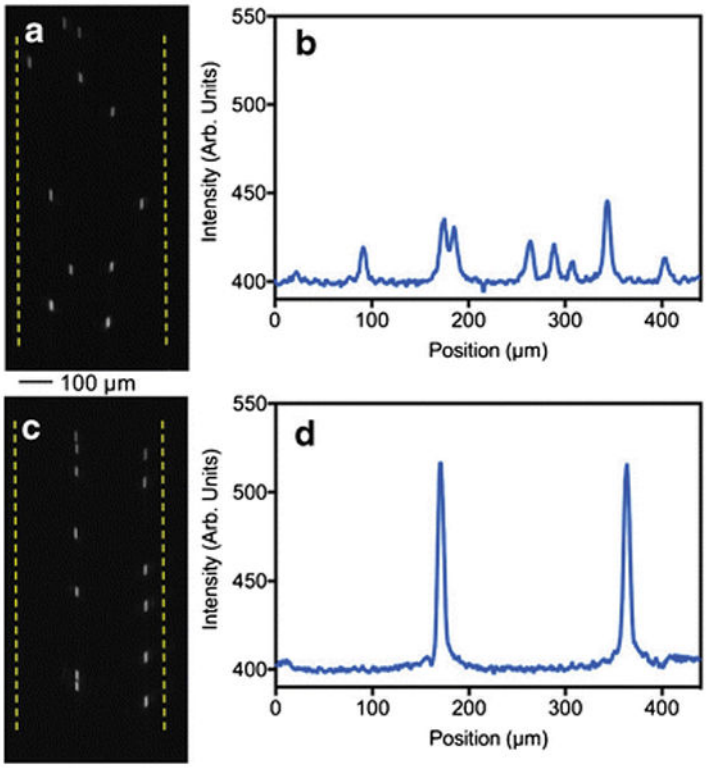

Fig. 6.

Epi-fluorescence micrographs and the plot profile image scanning showing the multinode focusing of polystyrene microsphere in the Al device (width = 440 μm). Non-focused streams of particles (a) and the plot profile scanning of the image (b). Microspheres are focused in to two streams (c and d).